Richardson Number Statistics in the Seasonal Thermocline

LAURIE PADMAN

Marine Studies Centre, University of Sydney, Sydney 2006, Australia

IAN S. F. JONES

RAN Research Laboratory, Darlinghurst, NSW 2010, Australia

(Manuscript received 7 August 1984, in final form 12 February 1985)

ABSTRACT

Statistics of Richardson number in the seasonal thermocline are determined for a simple model and from experiments over the continental shelf. The model consists of normally distributed and uncorrelated density gradient and shear (such as may be caused by an internal wave field) plus a mean shear. It is shown that the most probable Richardson number may be much lower than the Richardson number based on the mean density gradient and shear.

The distributions of Richardson number for two experiments in the seasonal thermocline in Bass Strait, between mainland Australia and Tasmania, are determined from a probe that samples velocity and temperature differences at 1 Hz, over vertical separations of 1 m. Away from surface wave frequencies the data are shown to be adequately described by the above model. In both interfaces significant shear energy occurs above the maximum Brunt-Väisälä frequency of about 0.01 Hz. Judged by the temperature inversions of scales greater than one meter that were observed within the less stable interface, this shear variance leads to Richardson numbers that are subcritical for significant periods.

1. Introduction

Determining the rate of entrainment across the seasonal thermocline of the world oceans is important in many problems involving the heat balance of the upper ocean and the prediction of depth of the surface mixed layer. At present there are a number of expressions which attempt to relate the rate of deepening of the mixed layer to the external variables believed to be important. Mixed layer depth, density gradient in the thermocline and surface wind stress are obvious candidates. To look more closely at these relationships, laboratory studies have been made of entrainment rates due to turbulence in the layer above the thermocline (so called grid-stirred experiments such as that by Rouse and Dodu, 1955) and by both turbulence and mean shear, e.g., Kato and Phillips (1969). In recent papers by Deardorff and Willis (1982) and Jones and Mulhearn (1983) the relative influence of external turbulence and mean shear in determining the rate of entrainment is clarified.

In the ocean tentative progress has been made in describing the mean velocity and density profiles through a seasonal thermocline by Jones (1983). Here the gradient Richardson number from the "mean profiles" was determined and entrainment direction predicted from the asymmetry of the thermocline. What is not known is how to relate the mean Richardson number profiles to the external variables or how to relate the rate of entrainment to the Richardson number derived from these mean quantities. In the present paper it is this latter problem that motivated us to study the statistics of the Richardson number within the seasonal thermocline over a portion of the continental shelf.

Previous studies of the statistics of Richardson number have focused on the main oceanic thermocline, in which the shear variance is dominated by the internal wave field. Desaubies and Smith (1982) showed that a model in which the two components of shear and the temperature gradient are normally distributed and uncorrelated random variables, with variances related by the Garrett and Munk (1975) "universal" internal wave spectrum, adequately represented their observed Richardson number distributions. Toole and Hayes (1984) showed further that a skewed temperature gradient distribution as predicted by Desaubies and Gregg (1981), significantly improved the fit between an internal wave-field model and data from the main thermocline in the eastern equatorial Pacific.

In the present study, however, there is no reason to suspect *a priori* that these models would be applicable. In Bass Strait the seasonal thermocline is located between two fairly well mixed layers, one stretching to the sea surface and the other, as a result of tidal stirring, to the sea floor. While a broad range

of internal wavelike motions have been observed in the study region (e.g., Jones and Padman, 1983), shear within the thermocline may also be attributed to other mechanisms such as the upper mixed-layer response to wind forcing, and the large-scale turbulence of the surrounding mixed layers. Therefore, rather than constraining the variances and spectral shapes to conform to the Garrett and Munk model, we shall consider a number of possible shear and density gradient variances and compare the derived Richardson number statistics with our data.

Following a discussion of the experimental procedure we review the elementary statistics to compute the probability distribution of the Richardson number from assumed distributions of velocity and density gradients. Next we compare this calculation with statistics collected with a Richardson number probe during two summer deployments from oil platforms in Bass Strait.

2. Equipment

The data were collected from the Kingfish B and Barracouta oil and gas platforms in eastern Bass Strait (Fig. 1). The locations are as follows;

Kingfish B: 38°36'S, 148°11'E (water depth 78 m)
Barracouta: 38°18'S, 147°40.5'E (water depth 48 m).

Both platforms are instrumented with automatically recording thermistor chains so that the short-duration Richardson number probe results can be related to the longer term variability in the thermal structure.

The Richardson number probe (RNP) is described by Jones and Bruzzone (1981) and a diagram of the unit is shown in Fig. 2. The probe is designed to measure instantaneous vertical gradients of temperature and horizontal velocity so that the gradient Richardson number can be estimated. The design is

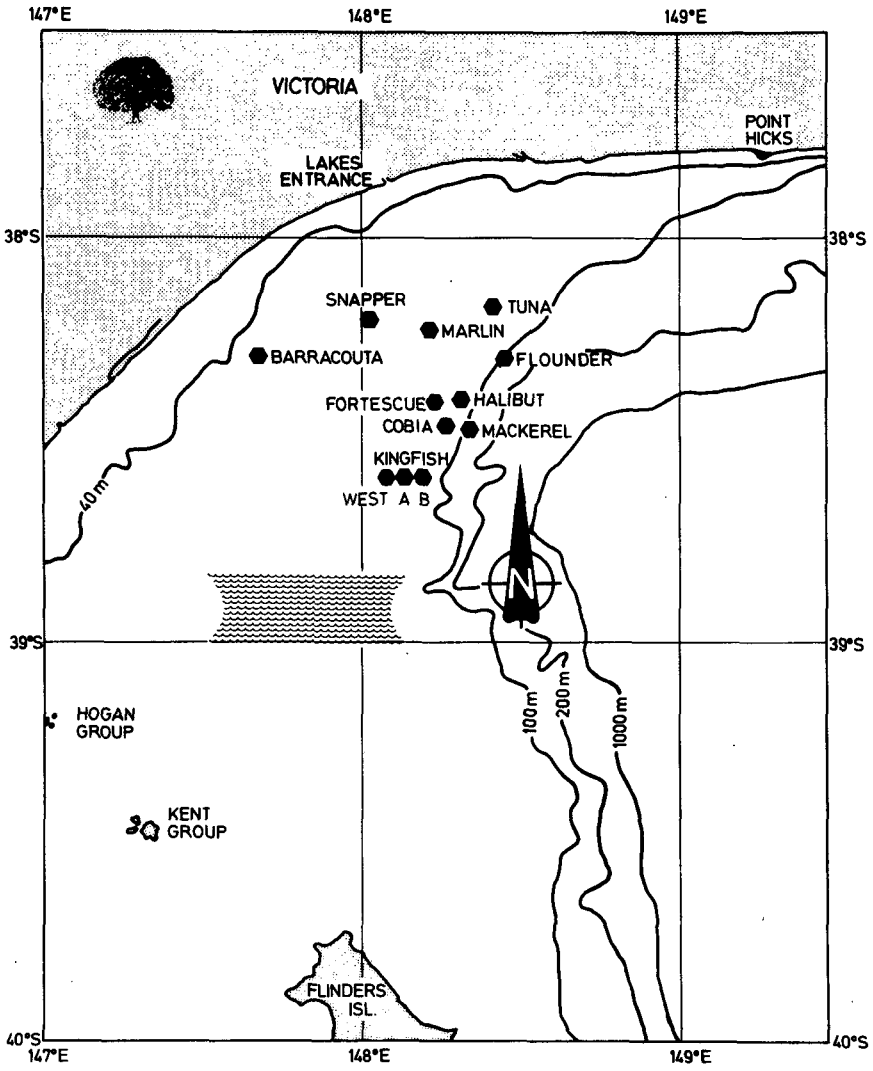

FIG. 1. Platform locations in eastern Bass Strait.

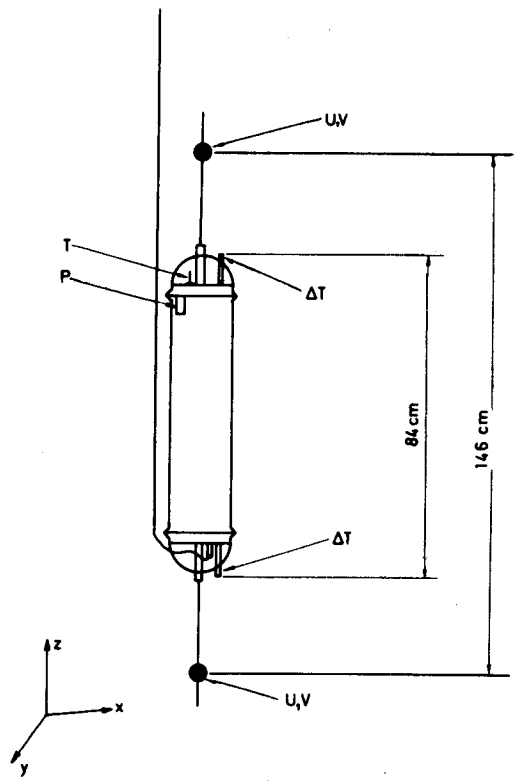

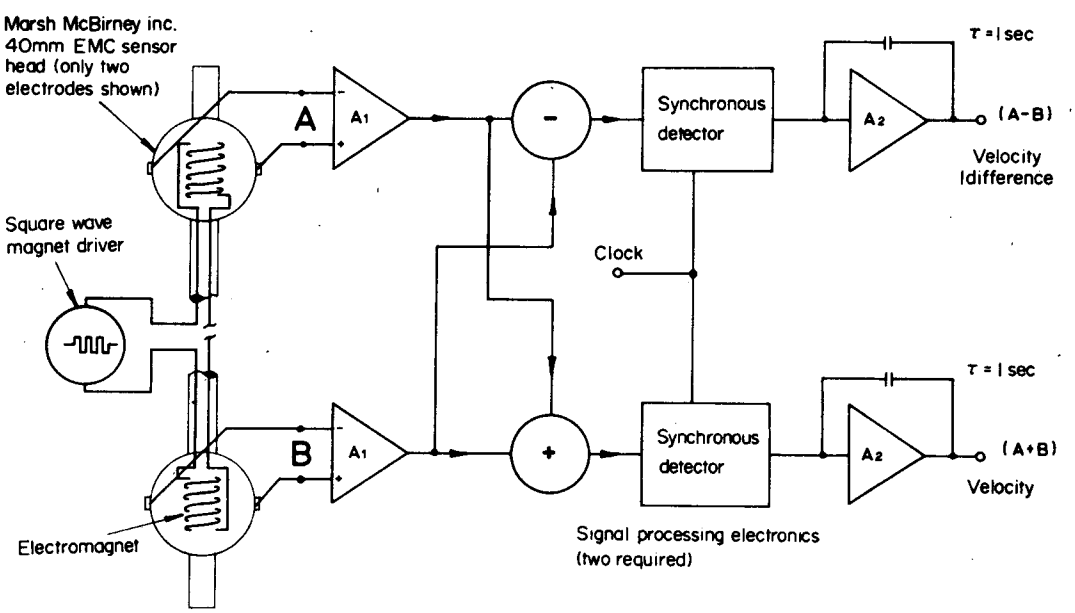

FIG. 2. Richardson number probe (after Jones and Bruzzone, 1981).

constrained by noise limitations on the electromagnetic current sensors and by the expected vertical length scales for oceanic density and currents. Vertical structure exists down to the Kolmogorov microscale $l_k = (\nu^3/\epsilon_0)^{1/4}$ where ν is the kinematic viscosity (10^{-6} m^2 s^{-1}) and ϵ_0 is the dissipation rate of turbulent kinetic energy, estimated by Gargett and Osborn (1981) to be of order 10^{-7} m^2 s^{-3} in the upper mixed layer of the ocean. Hence l_k is of order 1 mm in the mixed layers. Velocity differences at these vertical scales are too small to detect at present by a device collecting a time series at a fixed sensor separation. The minimum separation must be large enough such that the velocity differences that make up the shears being studied exceed the instrument noise which in our case is about 1 cm s^{-1}. Typical shears in the upper ocean, such as shear due to surface waves and direct wind-forcing, have magnitudes of about 0.01 s^{-1}. A sensor separation of greater than 1 m is therefore required.

A feature of the RNP is that the coils for both velocity sensors are driven by the same current, so that any instability in the magnet power supply has the same effect on both. No-flow bucket calibrations give instrument noise levels of 0.15 cm s^{-1} for each current channel, and 0.002 s^{-1} for each shear channel. The instrument resolution is however limited by fluid mechanical problems such as flow noise around the sensors and shears induced by package tilt, rather than the electronic noise.

The RNP also includes orientation sensors to determine the degree of contamination of shear measurements by package tilt, and a compass with a time constant of about 0.5 s, sufficient to resolve probe rotations caused by surface waves. The data from the RNP are cabled to a surface data-acquisition package to enable real time analysis. The output voltages are recorded digitally on to magnetic tape, and selected channels are displayed on a strip chart recorder.

RNP data were collected during February 1981 and again in February 1982 during times when the mean flow placed the instrument, deployed from the southern side of the platform, upstream of the platform legs. Other RNP experiments have been discussed by Jones and Bruzzone (1981).

3. Review of statistics

Assuming that the temperature and velocity gradients in a stratified fluid are normally distributed and uncorrelated, we can calculate the probability distribution of the Richardson number. We will examine the applicability of these assumptions for the seasonal thermocline over the continental shelf in the next section.

We assume that $\delta T/\delta z = T_z$ is distributed as

$$P(T_z \leq T_z') = \frac{1}{\sigma_{T_z}\sqrt{\pi}} \int_{-\infty}^{T_z'} \exp\left(-\frac{(V - \bar{T}_z)^2}{2\sigma_{T_z}^2}\right) dV$$

where $\bar{T}_z$ is the mean temperature gradient and σ_{T_z} is the standard deviation of the temperature gradient. Similarly there will be a mean velocity gradient in the east direction $\bar{U}_z$ and the north direction $\bar{V}_z$ (right hand convention with z upward).

If we assume that all three quantities, T_z, V_z and U_z, are statistically independent, then by Monte Carlo simulation we can calculate the probability distribution of the Richardson number

$$\mathrm{Ri} = \frac{g\alpha}{\rho} \frac{T_z}{U_z^2 + V_z^2}$$

where α is the relationship between density gradient and temperature gradient. We will assume that salinity gradients are not important or that the T–S relationship can be linearized. The Richardson number based on mean quantities is defined as

$$\overline{\mathrm{Ri}} = \frac{g\alpha}{\rho} \frac{\bar{T}_z}{\bar{U}_z^2 + \bar{V}_z^2}.$$

Since it is possible to find a direction in which one component of mean shear is zero we will neglect $\bar{V}_z$ and assume for the moment that the shear fluctuations are horizontally isotropic, i.e., $\sigma_{U_z} = \sigma_{V_z}$. Now we can consider the problem as a function of $\overline{\mathrm{Ri}}$, $\bar{T}_z$, $\bar{U}_z$, σ_{T_z} and σ_{U_z}.

We now nondimensionalize these variables by defining $T_z^* \equiv T_z/\bar{T}_z$, $U_z^* \equiv U_z/\bar{U}_z$, $\sigma_{U_z}^* \equiv \sigma_{U_z}/\bar{U}_z$, $V_z^* \equiv V_z/\bar{U}_z$, $\sigma_{V_z}^* \equiv \sigma_{V_z}/\bar{U}_z$ and $\sigma_{T_z}^* \equiv \sigma_{T_z}/\bar{T}_z$, such that $\bar{T}_z^* = \bar{U}_z^* = 1$, $\bar{V}_z^* = 0$ and define $\mathrm{Ri}^* \equiv T_z^*/(U_z^{*2} + V_z^{*2})$. Then it follows that

$$\overline{\mathrm{Ri}}^* = \bar{T}_z^*/(\bar{U}_z^{*2} + \bar{V}_z^{*2}) = 1.$$

Figure 3 shows the statistical distribution of Ri* as the nondimensional rms temperature gradients and velocity gradients are varied while $\overline{\mathrm{Ri}}^*$ calculated from the means remains constant at unity. Figure 3 may be regarded as a Richardson number distribution by noting that $\mathrm{Ri} = \mathrm{Ri}^* \cdot \overline{\mathrm{Ri}}$. When $\sigma_{U_z}^*$ and $\sigma_{V_z}^*$ are zero, Fig. 3a–d, the Richardson number is distributed as the temperature, i.e., normally in the present model. The vertical columns in Fig. 3 show the influence of increasing velocity gradient variance while the horizontal rows show the influence of increasing the temperature gradient variance. Notice that as the velocity gradient variance increases, the modal (most common) value of the Ri* probability distribution becomes smaller, for example, Fig. 3a, 3e, 3j. This is an important point worth stressing, that although the Richardson number calculated from the mean values of density gradient and shear (i.e., $\overline{\mathrm{Ri}}$) remains constant, increasing the shear variance lowers the most probable Richardson number. Also note that as $\sigma_{U_z}^* \to \infty$, i.e. $\bar{U}_z \to 0$, the problem approaches that determined by Desaubies and Smith (1982). However, for the case of zero mean shear, $\overline{\mathrm{Ri}} = \infty$.

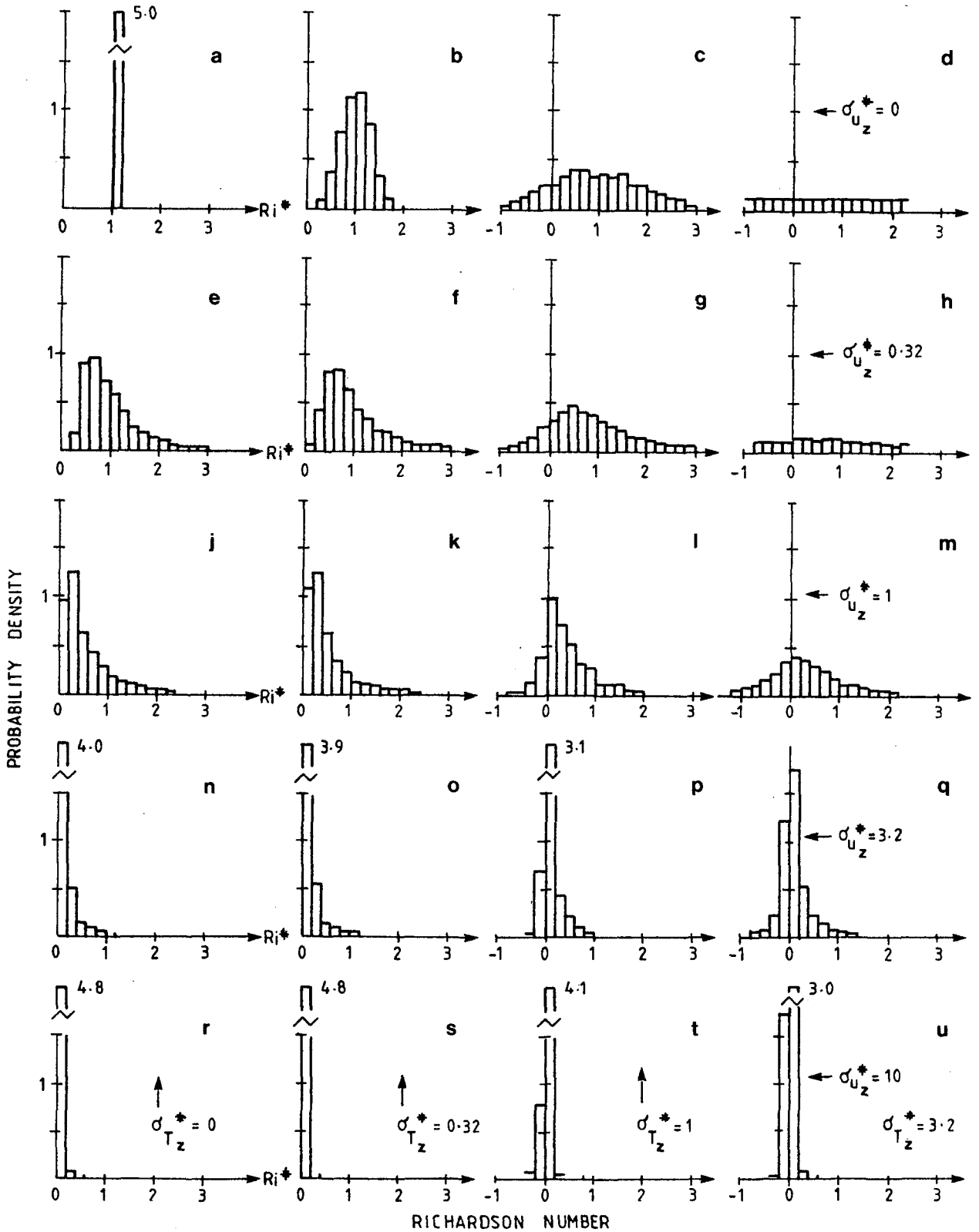

FIG. 3. Probability density of the Richardson number Ri* as a function of the nondimensional standard deviations $\sigma_{T_z}^*$, and $\sigma_{U_z}^*$ ($=\sigma_{V_z}^*$). Higher shear variances are lower in the figure.

4. Experimental results

The thermocline in Bass Strait may be affected by both the large-scale shears of the coastal ocean, thought of as mean shears, and by the turbulence of both mixed layers surrounding it. Two Richardson number probe (RNP) experiments, involving sampling of thermocline and mixed-layer temporal and spatial variability, are considered below. The sampling rate was 1 Hz, while temperature and current gradients were measured over vertical separations of about 1 m. A description of each experiment is given below and a summary is presented in Table 1.

a. RNP06 (Barracouta)

This record consists of three hours of data commencing at 1004 Eastern Standard Time (EST) on 26 February 1981 (Julian Day 057). The density profile is characterised by a thermocline of about 5.6°C in 3.4 m, at a mean depth of 20 m in 48 m of water. The bottom and surface currents are low (<0.08 m s^{-1}) with a mean current difference of 0.06 m s^{-1} between the mixed layers. A transient thermocline exists above the seasonal thermocline at a depth of about 10 m.

A series of "yo-yo" dips was made over one hour to define the average vertical structure shown in Fig. 4. The maximum temperature gradient of 2.2°C m^{-1} corresponds to a Brunt-Väisälä frequency of 0.01 Hz. The RNP was then left in the thermocline for two hours near the mean depth of the 17°C isotherm. Isotherm displacements were small so that no adjustments to the depth of the probe were necessary to maintain it within the thermocline.

Histograms of temperature gradient and velocity shear were calculated for this period and are shown in Fig. 5. The total shear variance, defined as the sum of the N/S and E/W variances, is 8.4×10^{-4} s.

The bulk Richardson number based on the 2048 s averages of temperature gradient and shear, was about 12.

b. RNP02 (Kingfish B)

This record consists of two hours of data commencing at 1040 EST on 10 February 1982 (Julian Day 041). The density profile is characterised by a broad thermocline, about 4.2°C in 18 m at a mean depth of 40 m in 78 m of water, and thermistor chain records show that a large-amplitude internal tide was present at this time. The bottom and surface currents are similar in magnitude at 0.30 m s^{-1} but have a significant angular shear between them, principally in the north component.

A measure of the mixed layer turbulence was made at a depth of 12 m followed by a measure of bottom layer turbulence, then 2400 seconds of data near the 16.5°C isotherm with the depth being adjusted to approximately follow the isotherm. The maximum Brunt-Väisälä frequency ($\Delta T/\Delta z_{max}$ = 0.8°C m^{-1}) was 6×10^{-3} Hz.

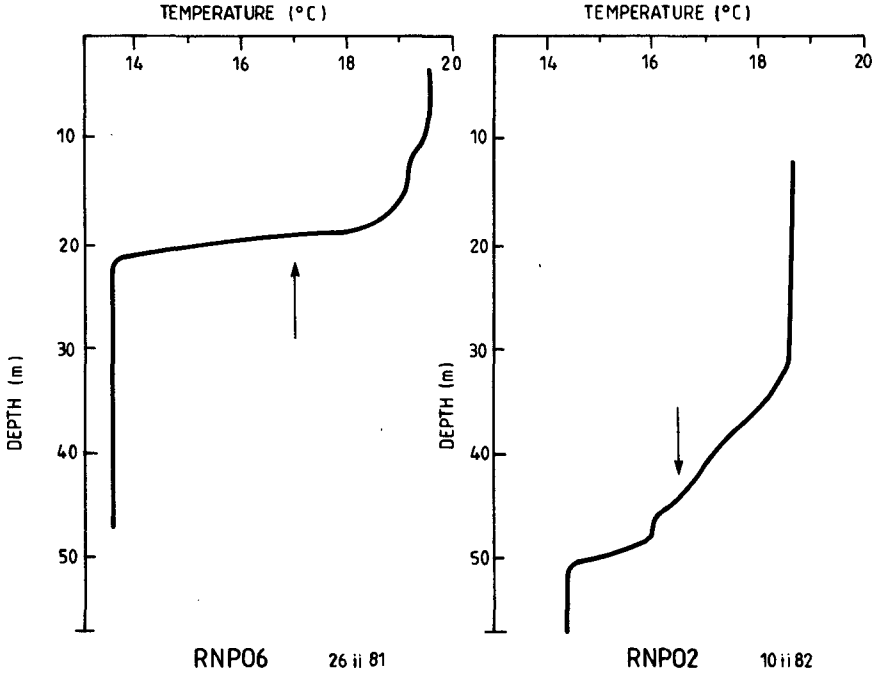

FIG. 4. Comparison of temperature–depth profiles from the Richardson number probe for two RNP experiments—RNP06 (26 February 1981) and RNP 02 (10 February 1982). The arrows indicate the approximate location of continuous sampling within the thermocline.

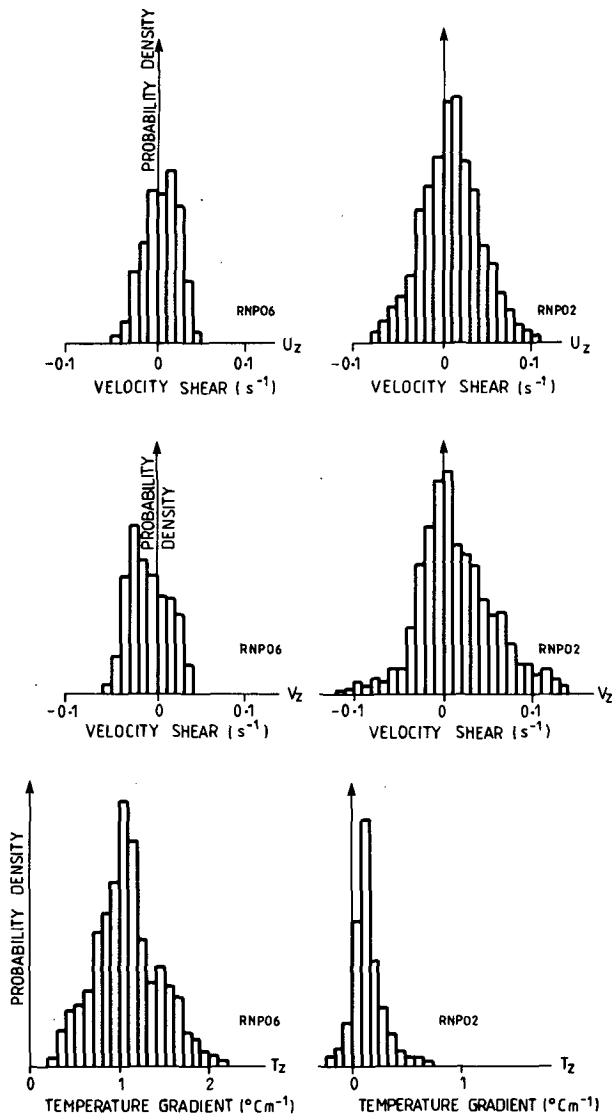

FIG. 5. The experimentally determined probability density for velocity gradient in the east direction, velocity gradient in north direction and temperature gradient, for RNP06 (26 February 1981) and RNP02 (10 February 1982).

Histograms of the temperature gradient and the two components of velocity gradient are shown in Fig. 5. It is notable that about 6% of this record has negative temperature gradients of up to $-0.3°C\ m^{-1}$. This indicates active turbulence on length scales greater than or equal to the sensor separation of 0.84 m.

The bulk Richardson number based on the 2048 s averages of temperature gradient and shear, was about 4.

5. Discussion

Figure 6 shows the Richardson number distributions, scaled by the mean Richardson numbers, for the two experiments RNP06 and RNP02. Note that although RNP06 is dominated by scaled Richardson numbers of 0 to 0.2, because the mean Richardson number is high (16) there are actually no occurrences of $Ri < 0.25$. Therefore, we do not expect turbulence to develop on scales equal to or greater than 1 m. As expected from the non-dimensionalised rms shears and temperature gradient in Table 1, the distribution most closely approximates Fig. 3o.

The distribution of Richardson number for RNP02 most nearly approximates Fig. 3p, again as expected from the nondimensionalized shear and temperature gradient variances (Table 1). Note that $\overline{Ri}$ (=1.3) is the mean Richardson number based on the shears and temperature gradients measured by the probe, and is smaller than the bulk Richardson number for the entire interface, based on velocity and density differences between the mixed layers. The occurrence of negative Richardson numbers strongly suggests active turbulence on scales of 1 m or greater. The reduced probability of negative Richardson number observed, compared with Fig. 3p, presumably reflects the lack of physics in the simulation, i.e., the collapse of a gravitational instability is not modeled.

RNP02, as well as inversions, also has a high probability of subcritical (<0.25) Richardson number in the 1 s averaged data. However it is not appropriate to infer from this that turbulence is likely to be generated. For a given vertical length scale of an instability, a finite time is required for the instability to become gravitationally unstable. If the shear is removed before this time elapses, the interface gradually relaxes through viscous-damped buoyancy oscillations without turbulence, to its initial state. It is therefore necessary to consider some average of the Richardson number to define the interface that becomes turbulent. We define a time-averaged Richardson number by

$$\langle \mathrm{Ri} \rangle_t = \frac{g\alpha}{\rho} \frac{\langle \Delta T/\Delta z \rangle_t}{\langle \Delta U/\Delta z \rangle_t^2 + \langle \Delta V/\Delta z \rangle_t^2}$$

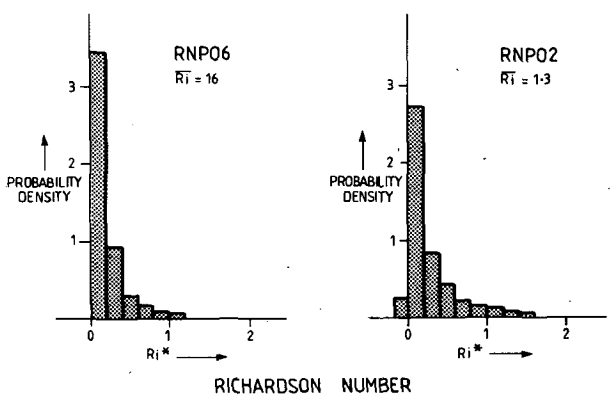

FIG. 6. Scaled Richardson number ($Ri^* = Ri/\overline{Ri}$) distributions for the two experiments RNP06 (26 February 1981) and RNP02 (10 February 1982).

TABLE 1. Summary of Richardson number probe experiments.

	26 February 1981	10 February 1982
Name	RNP06	RNP02
Water depth (m)	48	78
Sensor depth (m)	18	51
Wind speed (m s^{-1})	12.4	8.9
Significant wave height (m)	2.2	1.1
Mean current (m s^{-1})	0.02	0.31
Shear variance, $\sigma_{U_z}^2$ (s^{-2})	8.4×10^{-4}	31.4×10^{-4}
$\sigma_{U_z}/\bar{U}_z$	3	3
Temperature variance, $\sigma_{T_z}^2$ [(°C)^2]	0.14	0.039
$\sigma_{T_z}/\bar{T}_z$	0.3	1
Mean Richardson number $\left(\overline{\mathrm{Ri}} = \frac{g\alpha}{\rho}\frac{\bar{T}_z}{\bar{U}_z^2}\right)$	16	1.3
Bulk Properties of the Thermocline		
Current difference (m s^{-1})	0.055	0.235
Temperature difference (°C)	5.6	4.2
Thermocline thickness (m)	3.5	17.5
Bulk Richardson number	12	4

where $\langle\ \rangle_t$ implies a temporal average over time t. It follows that $\langle \mathrm{Ri} \rangle_{t\to\infty} = \overline{\mathrm{Ri}}$.

The effect of temporal averaging is shown in Fig. 7, for a period of record commencing at 1200 EST from RNP02. This figure is a time series plot of temperature gradient, shear magnitude and Richardson number for both the "unfiltered" (1 s) and 150 s low-passed data. The choice of cut-off period is based on the Thorpe (1973) time scale for Kelvin-Helmholtz instabilities growing across the entire interface. While turbulence may develop on shorter time scales over smaller vertical scales, a local catastrophic failure of the interface, that is, one in which upper and lower mixed layer waters mix directly, should only occur if the Richardson number remains below the critical value for longer than this time. The probability distributions of temperature gradient and absolute values of north and east shear for the above record are shown in Fig. 8.

By examining the power density spectra of both T_z and U_z it can be seen at which cutoff frequency f_c filtering may have a significant effect, noting that the variance of filtered T_z is given by

$$\sigma_{T_z}^2 = \int_0^{f_c} \Phi_{T_z}(f)\,df$$

where $\Phi_{T_z}(f)$ is the power spectral density at frequency f of T_z (and similarly for $\sigma_{U_z}^2$).

The power density spectra of temperature gradient and shear within the thermocline are shown in Figs. 9 (RNP06) and 10 (RNP02). While in RNP02 no significant peak is visible, during RNP06 there is significant energy near 0.1 Hz, apparently surface wave shear. In either case, however, it is obvious that the choice of filtering frequency will affect the resultant Richardson number distribution by reducing the total variance without altering the Richardson number based on the mean gradients $\overline{\mathrm{Ri}}$. Decreasing the cut-off frequency decreases the shear variance, which, as we have already seen in Fig. 3, leads to a less skewed Richardson number distribution with the mode approaching the mean Richardson number. These results are independent of the spectral shape but assume normally distributed, uncorrelated variables. While not satisfying the χ^2-test at the 90% level, the normal distribution appears an adequate representation for the majority of the histograms of Fig. 5. The correlations between variables are low, ranging from 0.04 to 0.22, the latter value being between the north and east components of shear for RNP06, and is due to the high surface wave energy in this record. As can be seen from the coherence plots in Figs. 9 and 10, between temperature gradient and shear, the coherences are not in general statistically significant at the 95% level. This result is in agreement with both internal wave models, applicable to the frequency band from the Coriolis frequency ω_e to $N_{\max}$, and turbulence ($f > N_{\max}$).

The effect of filtering is illustrated by the RNP02 experiment. By filtering at 0.01 Hz, similar to the Kelvin-Helmholtz instability time scale, the ratio of rms to mean shear decreases from $\sigma^*_{U_z} = 3.4$ to 1.1, while $\sigma^*_{T_z}$ decreases from 1 to 0.5. Therefore the distribution of Richardson number for the filtered variables approximates Fig. 3k rather than Fig. 3p, i.e. a much broader distribution. This is accompanied by a decrease in the probability of unstable Richardson number. Note that this probability is a function of $\sigma^*_{U_z}$, $\sigma^*_{T_z}$ and $\overline{\mathrm{Ri}}$, the Richardson number based on the means $\bar{U}_z$ and $\bar{T}_z$. Then from the definition of Ri*, the relationship

$$\Pr(\mathrm{Ri} < \mathrm{Ri}_{\mathrm{crit}}) = \Pr(\mathrm{Ri}^* < \mathrm{Ri}_{\mathrm{crit}}/\overline{\mathrm{Ri}})$$

can be used to interpret Fig. 3.

A comparison may be made with the observations by Evans (1982) (using free-fall probes through the oceanic thermocline), who showed that there existed a nonzero probability of unstable Richardson number ($\mathrm{Ri} < 0.25$) in a field with a stable bulk Richardson number of order 1. Evans also showed that the effect of doubling the vertical averaging interval from 1.1 to 2.2 m was roughly to halve $\Pr(\mathrm{Ri} < 0.25)$, comparable with the present result that to increase the averaging time is to lower the probability of small Richardson number.

6. Causes of velocity gradient variance

While the temperature gradient variance is of some significance, the most important quantity in determining the difference between the mode of the Richardson number probability distribution and the mean Richardson number is the velocity gradient variance. The causes of velocity gradient variance are unclear at this time but because they extend to frequencies

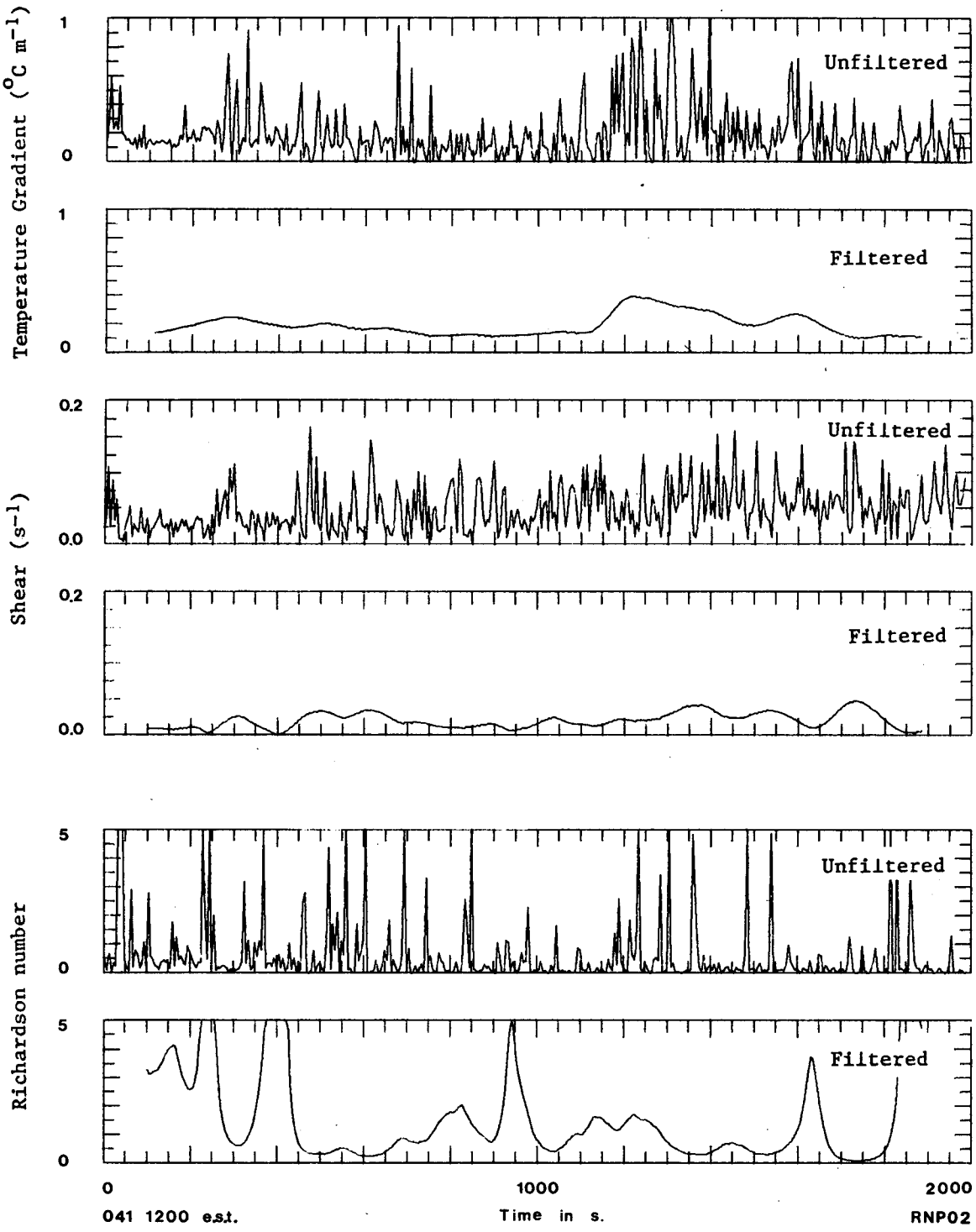

FIG. 7. Time series of unfiltered and 150 s low-pass filtered temperature gradient, shear magnitude and Richardson number from RNP02 (10 February 1982). Note that the "filtered" Richardson number $\langle Ri \rangle$ is a function of filtered shear and temperature gradients.

above the maximum Brunt-Väisälä frequency they cannot all be attributed to free internal waves of the type modeled by Desaubies and Smith (1982). While surface waves contribute to the shear energy near 0.1 Hz there remains a considerable amount of shear between the surface and free internal-wave frequency bands. This shear may be due to either the turbulence of the external mixed layers, or a turbulent energy cascade from a low-frequency instability. The role of mixed layer turbulence in generating shear within the

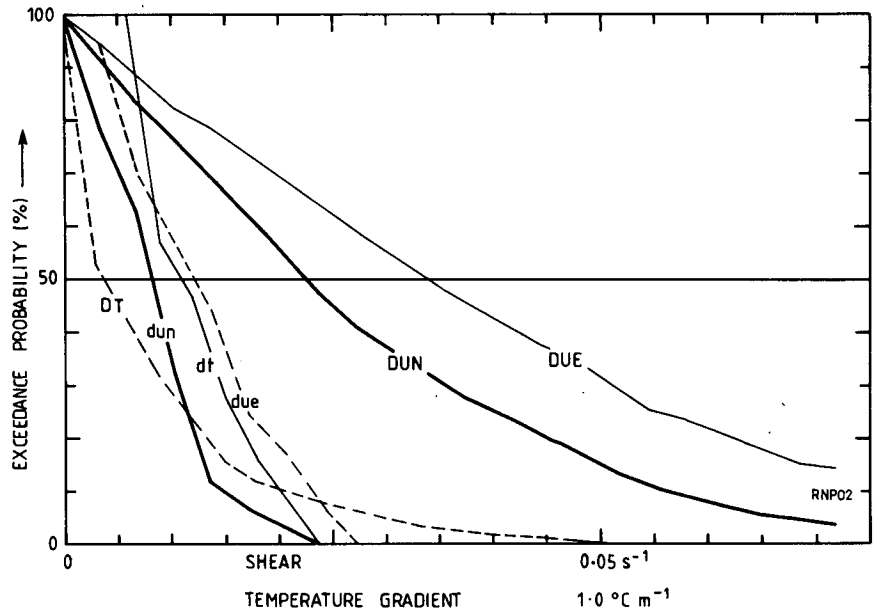

FIG. 8. Probability of exceedence of N/S and E/W shears and temperature gradient from RNP02 (10 February 1982), showing unfiltered (DUN, DUE, DT) and 150 s low-pass filtered (dun, due, dt) distributions.

thermocline is unclear. However for typical boundary shear stresses the friction velocities defined as $u_* = (\tau/\rho)^{1/2}$ of both layers are about 0.02 m s^{-1}. Then for a thermocline of 4 m thickness, the shears imposed by the mixed layer turbulence are of order 0.01 s^{-1}. Further, the time scales of the turbulent velocity

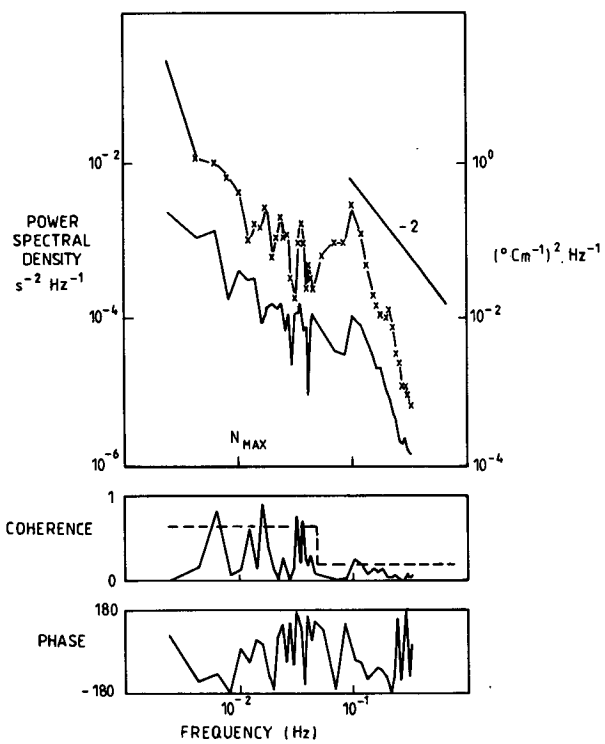

FIG. 9. Power spectral densities of shear (solid line) and temperature gradient (cross-line), coherence-squared and relative phase for measurements made within the thermocline during RNP06. 95% confidence limits are shown as broken lines.

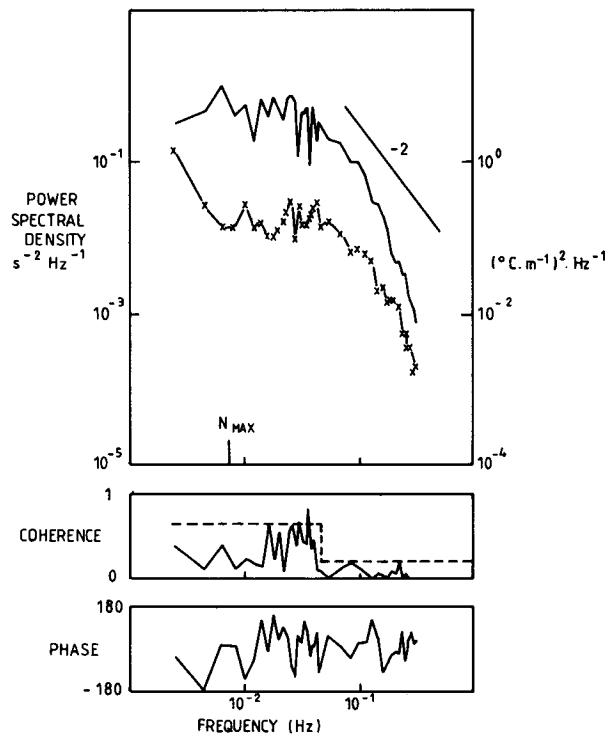

FIG. 10. Power spectral densities of shear (solid line) and temperature gradient (cross-line), coherence-squared and relative phase for measurements made within the thermocline during RNP02. 95% confidence limits are shown as broken lines.

fluctuations in the mixed layers may be approximated by

$$t_{ml} = H/\bar{U}$$

where H is the mixed-layer thickness and $\bar{U}$ is the mean velocity of the mixed layer (ml) past the observer. This assumes that the large eddies fill the mixed layer and are advected by the mean current at $\bar{U}$ past the stationary probe. For a 30-m-thick layer and a mean flow of 0.30 m s^{-1}, t_{ml} is about 100 s. A fluctuating velocity gradient is therefore established between the two turbulent mixed layers, with time scales set by the scales of the mixed layers. For a sufficiently thin thermocline and large u_* in one or both of the mixed layers, these shears may result in periods of Richardson number low enough to induce intermittent turbulence in the interface.

If the shear fluctuations we observed were dependent only on the vertical displacement of the probe from some reference isotherm and not on time, then vertical advection of the thermocline past the probe such as caused by a mode 1 internal wave, would be seen as a time-dependent shear. The shear variance for small ranges of temperature (i.e., small ranges of depth relative to the reference level) was calculated, and showed that the fluctuations in measured shear were dominated by time-dependence rather than relative depth-dependence. That is, we are not merely recording the variation in shear due to the varying position of the RNP within the thermocline.

7. Conclusions

For Gaussian statistics we have shown that the probability density function of Richardson number depends upon the ratio of rms to mean shear $\sigma^*_{U_z} = \sigma_{U_z}/\bar{U}_z$ and similarly $\sigma^*_{T_z} = \sigma_{T_z}/\bar{T}_z$. In particular as the shear variance $\sigma^*_{U_z}$ increases, the modal Richardson number decreases from a maximum of the mean Richardson number when $\sigma_{U_z} = 0$. The probability of occurrence of subcritical Richardson number is a function of $\sigma^*_{U_z}$, $\sigma^*_{T_z}$ and the mean Richardson number. The two time series of Richardson number measured in the seasonal thermocline in Bass Strait support the use of uncorrelated Gaussian statistics for U_z and T_z.

If we accept that periods of low Richardson number can occur on space and time scales shorter than those that are chosen to define the external extent of the sheared flow being studied, then the prospect of defining the probability of turbulence occurring and a rate of entrainment, in terms of mean Richardson number, recedes. We expect to need to know, as well as the mean Richardson number, at least the shear variance in order to parametrize the order of entrainment.

From observations it has been shown that significant shear fluctuations occur at all frequencies up to the surface wave frequencies. Thus it is not appropriate to model the Richardson number fluctuations as the result of free internal waves for the coastal ocean. The shear energy at frequencies above the maximum Brunt-Väisälä frequency may be caused either directly by the turbulent velocity fluctuations of surrounding mixed layers, or by the turbulent energy cascade from lower-frequency motions. For a probe with a fixed sensor separation Δz, the integral scale of the instability must be inferred from the Richardson number statistics: if no subcritical Richardson numbers are observed, this scale should be smaller than Δz, while if the probability of low Richardson number is nonzero, the vertical scale of dynamically unstable structures should be greater than Δz, as was observed in RNP02, where the temperature gradient was negative for 6% of the record. In the former case the shear results from uncorrelated smaller-scale vortices at each sensor.

The effect of filtering of temperature and velocity gradients prior to calculating the Richardson number probability density function for situations where these gradients have red spectra is critically dependent on the cutoff frequency chosen. Since filtering does not affect the Richardson number calculated from the mean quantities, the change in cutoff frequency can be modeled by a change in $\sigma^*_{U_z}$ and $\sigma^*_{T_z}$. Thus the probability of a critical Richardson number occurring for a chosen time scale, can be assessed from Fig. 3.

Acknowledgments. We wish to thank ESSO-BHP for allowing us to make measurements over a number of years from their Bass Strait platforms.

REFERENCES

Deardorff, J. W., and G. E. Willis, 1982: Dependence of mixed-layer entrainment on shear stress and velocity jump. *J. Fluid Mech.*, **115**, 123–149.

Desaubies, Y., and M. C. Gregg, 1981: Reversible and irreversible fine structure. *J. Phys. Oceanogr.*, **11**, 541–556.

——, and W. K. Smith, 1982: Statistics of Richardson Number and instability in oceanic internal waves. *J. Phys. Oceanogr.*, **12**, 1245–1259.

Evans, D. L., 1982: Observations of small scale shear and density structure in the ocean. *Deep-Sea Res.*, **29**, 581–595.

Gargett, A. E., and T. R. Osborn, 1981: Small scale shear measurements during the Fine and Microstructure Experiment (FAME). *J. Geophys. Res.*, **86**, 1929–1944.

Garrett, C., and W. H. Munk, 1975: Space-time scales of internal waves: A progress report. *J. Geophys. Res.*, **80**, 291–297.

——, 1983: Richardson number profiles over the continental shelf. *J. Phys. Oceanogr.*, **13**, 1829–1835.

Jones, I. S. F., and F. Bruzzone, 1981: An oceanographic Richardson number probe. *Deep-Sea Res.*, **28A**, 507–519.

——, and P. J. Mulhearn, 1983: The influence of external turbulence on sheared interfaces. *Geophys. Astrophys. Fluid Dyn.*, **24**, 49–62.

——, and L. Padman, 1983: Semi-diurnal internal tides in Eastern Bass Strait. *Aust. J. Mar. Freshwater Res.*, **34**, 159–172.

Kato, H., and O. M. Phillips, 1969: On the penetration of a turbulent layer into stratified fluid. *J. Fluid Mech.*, **37**, 643–655.

Rouse, H., and J. Dodu, 1955: Diffusion turbulente a travers une discontinuite de densite. *La Houille Blanche*, **4**, 522–532.

Thorpe, S. A., 1973: Experiments on instability and turbulence in a stratified shear flow. *J. Fluid Mech.*, **33**, 639–656.

Toole, J. M., and S. P. Hayes, 1984: Finescale velocity-density characteristics and Richardson number statistics of the Eastern Equatorial Pacific. *J. Phys. Oceanogr.*, **14**, 712–726.